Boundary-Layer Meteorol (2013) 147:421–441
DOI 10.1007/s10546-012-9789-3

ARTICLE

Resolved Versus Parametrized Boundary-Layer Plumes. Part III: Derivation of a Statistical Scheme for Cumulus Clouds

A. Jam · F. Hourdin · C. Rio · F. Couvreux

Received: 19 July 2012 / Accepted: 27 November 2012 / Published online: 21 December 2012

Abstract We present a statistical cloud scheme based on the subgrid-scale distribution of the saturation deficit. When analyzed in large-eddy simulations (LES) of a typical cloudy convective boundary layer, this distribution is shown to be bimodal and reasonably well-fitted by a bi-Gaussian distribution. Thanks to a tracer-based conditional sampling of coherent structures of the convective boundary layer in LES, we demonstrate that one mode corresponds to plumes of buoyant air arising from the surface, and the second to their environment, both within the cloud and sub-cloud layers. According to this analysis, we propose a cloud scheme based on a bi-Gaussian distribution of the saturation deficit, which can be easily coupled with any mass-flux scheme that discriminates buoyant plumes from their environment. For that, the standard deviations of the two Gaussian modes are parametrized starting from the top-hat distribution of the subgrid-scale thermodynamic variables given by the mass-flux scheme. Single-column model simulations of continental and maritime case studies show that this approach allows us to capture the vertical and temporal variations of the cloud cover and liquid water.

Keywords Boundary-layer thermals · Cloud scheme · Conditional sampling · Large-eddy simulations · Probability distribution function

1 Introduction

In climate or numerical weather prediction models, parametrizations of cloudiness are often based on a priori distributions of subgrid-scale variables from which cloud cover is deduced as a fraction of the mesh for which saturation is exceeded. For example, Bougeault (1981) introduced a skewed exponential distribution of total water, while Smith (1990) proposed a

A. Jam (✉) · F. Hourdin · C. Rio
LMD-IPSL, 4 pl Jussieu, 75005 Paris, France
e-mail: ajlmd@lmd.jussieu.fr

F. Couvreux
GAME Meteo-France and CNRS, 42 Coriolis, 31057 Toulouse, France

triangular distribution of relative humidity. Bony and Emanuel (2001) and Tompkins (2002) proposed respectively unimodal log-normal and beta distributions of total water. A key issue is the computation of the higher-order moments of the distributions, which can be derived either directly as a function of the thermodynamical mean state variables or coupled to the parametrization of turbulence (Golaz et al. 2002a) or convection (Bony and Emanuel 2001).

Regarding cumulus clouds, several studies have shown, using observations or large-eddy simulation (LES), that bi-Gaussian distributions fit reasonably well the skewed and bi-modal shapes commonly observed in the convective boundary layer (CBL) (Lewellen and Yoh 1993; Larson 2002). Since then, statistical cloud schemes based on bi-Gaussian joint probability density functions (PDF) of several variables such as vertical velocity, liquid potential temperature or total water have been proposed (Golaz et al. 2002a; Neggers 2009). For the computation of the moments of the PDFs, Golaz et al. (2002a) use a higher-order turbulence closure scheme, shown to be successful for a variety of regimes (Golaz et al. 2002b).

The skewness and bi-modality of the water distribution within the cumulus layer derives from the fact that the clouds are the saturated part of boundary-layer thermals initiated at the surface (Lemone and Pennell 1976). In the last decade, mass-flux schemes have been developed to represent the non-local vertical transport by these boundary-layer thermals. The combination of this mass-flux approach with a classical K-theory (Siebesma and Teixera, 2000; Hourdin et al., 2002; Soares et al., 2004; Rio and Hourdin, 2008; Pergaud et al., 2009; Neggers et al., 2009, among others) constitutes an alternative to the higher-order closure for the parametrization of the CBL. In this approach, the turbulent flux $\rho\overline{w'\Psi'}$ of a conservative variable Ψ, where ρ is the air density and X' is the turbulent fluctuation of a variable X, reads

$$\rho\overline{w'\Psi'} = -K\rho\frac{\partial\overline{\Psi}}{\partial z} + f\rho(\Psi_{\text{th}} - \overline{\Psi}), \tag{1}$$

where K is the turbulent diffusivity, f is the convective mass flux, $\overline{\Psi}$ is the large-scale value of Ψ, and Ψ_{th} its mean value in the subdomain of the mesh associated with updrafts. The convective mass flux f is given by

$$f = \rho\alpha w_{\text{th}}, \tag{2}$$

where α is the thermal fractional area and w_{th} is the mean vertical velocity within the thermals.

Several studies have proposed the coupling of a statistical cloud scheme with a boundary-layer mass-flux scheme. Following Bony and Emanuel (2001), Rio and Hourdin (2008) coupled their thermal plume model to a log-normal PDF of total water, the width of the distribution being diagnosed from the in-cloud thermal water content by an inverse procedure. With this approach, a reasonable cloud cover is obtained for both marine and continental fair-weather cumulus clouds. However, the maximum of cloud cover is generally simulated in the middle of the cloud layer whereas it should peak at cloud base. Neggers (2009) proposes to derive the standard deviations directly from cloudy updraft properties when coupling its mass-flux boundary-layer scheme (Neggers et al. 2009) with bi-modal joint PDFs of total water content and liquid potential temperature. According to Neggers (2009), the eddy-diffusivity/mass-flux decomposition implies a bimodal distribution of these two variables within a grid box, and thus decomposes the distribution into an updraft PDF and a diffusive PDF, the parameters of which are predicted in terms of mass-flux model parameters.

In the continuation of those studies, we propose here an alternative statistical cloud scheme based on the sum of two Gaussian functions. Here, one Gaussian function corresponds to the thermal plumes and the second to their environment. We use as a unique statistical variable the saturation deficit s, the most relevant variable to account for condensation processes

(Sommeria and Deardorff 1977; Lewellen and Yoh 1993; Chaboureau and Bechtold 2002; Larson 2002). The parameters of the two Gaussians can be computed directly from the "top hat" thermodynamical variables given by a mass-flux scheme of boundary-layer thermals. In order to evaluate the statistical scheme, we use LES that explicitly resolve coherent structures within the dry and cloudy CBL (Siebesma et al. 2003; Couvreux et al. 2005). The link between the resolved and parametrized boundary-layer thermal plumes is made through the tracer-based conditional sampling of Couvreux et al. (2010), which enables us to discriminate the thermal plumes resolved in the LES from their environment.

This study is part of the ongoing development of a new version LMDZ5B of the Laboratoire de M*é*t*é*orologie Dynamique global climate model (LMDZ). For that reason, we use a simple and efficient parametrization that reproduces satisfactorily shallow cumulus convection over both continent and ocean. The parametrization proposed here can be coupled to any mass-flux scheme of the boundary layer that provides thermodynamical variables within updrafts and their environment, as well as the coverage fraction of thermals.

In LMDZ5B, the statistical cloud scheme presented here is coupled to the thermal plume model of Rio and Hourdin (2008). This new set of parametrizations is evaluated here in a single column configuration of the LMDZ model for cases of cumulus convection. Long control and climate change simulations have since been performed as well with this LMDZ5B version in the frame of the CMIP5 exercise (Hourdin et al. 2012).

The paper is organized as follows: Sect. 2 presents an analysis of the water distribution in LES of two shallow convection cases, clearly attributing the two modes to the thermal plumes and their environment thanks to the tracer-based conditional sampling. A parametrization is proposed for the standard deviation of the two modes and is evaluated against LES results. In Sect. 3, the new statistical cloud scheme is implemented in the single-column version of LMDZ (LMDZ1D) and evaluated against LES.

2 Derivation of a New Statistical Cloud Scheme from LES

2.1 LES Case Studies

The derivation and evaluation of the new cloud scheme is based on a tracer-based sampling of LES of the Atmospheric Radiation Measurement (ARM) and Barbados Oceanographic Meteorological Experiment (BOMEX) case studies of shallow cumulus convection. The ARM case is derived from observations collected on June 21 1997 at the ARM site in Oklahoma, U.S.A. (Brown et al. 2002). This idealized case is typical of the diurnal cycle of shallow convection over land. BOMEX is a stationary case of shallow cumulus convection over the ocean, and took place on June, 22–30, 1969 (Holland and Rasmusson 1973; Siebesma et al. 2003). The case was built so as to produce undisturbed trade-wind convection under steady-state conditions.

The large-eddy simulations are performed with the Meso-NH non-hydrostatic model (Lafore et al. 1998), using a horizontal domain of 128×128 points with a horizontal resolution of 50 m, a vertical domain of 75 levels for BOMEX and 100 levels for ARM, with a resolution of 40 m and a timestep of 1 s.

The bi-Gaussian cloud scheme was since validated independently on a case of drizzling marine cumulus (Rico, Hourdin et al. 2012). Note that the availability of LES is central to the present study where we assess the internal variables of the parametrization scheme. It must be kept in mind however that the available LES cases, although generally selected to be representative of rather common situations, do not cover all the possible configurations of

boundary-layer clouds. Process scale assessment by comparison with LES must be accompanied by a global evaluation in the full three-dimensional model, by comparing for instance the simulated cloud cover or radiative effects with satellite observations, as done for the scheme presented here by Hourdin et al. (2012).

2.2 Resolved Versus Parametrized Boundary-Layer Thermals

In the mass-flux approach for the parametrization of the boundary layer considered here, the collective behaviour of a population of thermal plumes (or cells, or rolls) is represented through a unique thermal plume. In practice, the equations and free parameters of this "thermal plume parametrization" are derived and tuned so as to fit the collective behaviour of the population of updrafts resolved in a LES, which requires the discrimination of those resolved thermals from their environment.

We use for that an original conditional sampling introduced by Couvreux et al. (2010). In order to select in the LES the buoyant plumes that rise from the surface, this sampling makes use of a tracer emitted constantly at the surface and destroyed with a lifetime of 15 minutes. A grid point is supposed to belong to a thermal plume if its vertical velocity w is positive and if the difference between the tracer concentration and the mean concentration exceeds $m \times \sigma_{sv}$ (where σ_{sv} is the standard deviation of the tracer concentration at a given vertical level and m is a parameter). In the upper three quarters of the cloud layer, an additional criterion is applied to retain only the cloudy grid points ($q_c > 0$).

Couvreux et al. (2010) fix parameter m to a constant value of 1, while here m is fixed to 0.8 instead, which leads to a slightly better fit of the saturation deficit distribution with a bi-Gaussian PDF (not shown). The points selected by the sampling in the LES will be designated as "thermals" and the unselected points as the "environment".

2.3 Analysis of the Water Distribution

Following Sommeria and Deardorff (1977), Lewellen and Yoh (1993) or Chaboureau and Bechtold (2002), the saturation deficit s is used as the statistical variable. This variable quantifies the difference between the total specific humidity and that at saturation. Saturation deficit s can be expressed as a combination of the total specific humidity q_t and the specific humidity at saturation for liquid temperature T_l

$$s = a_l(q_t - q_{sat}(T_l)), \tag{3}$$

with,

$$a_l = \frac{1}{1 + q_{s_l} L_v / C_{pm}}, \tag{4}$$

where $q_{sat}(T_l)$ is the saturation at the liquid temperature, $T_l = T \exp(-q_l L_v / C_{pm} T)$, $q_{s_l} = 0.622\, q_{sat} L_v / R_d T_l^2$, q_l is the cloud liquid water, L_v is the latent heat of vaporization and C_{pm} is the heat capacity of moist air.

Figure 1c shows the s distribution obtained in the LES (bars) at hour 8 (1330 local time) of the ARM case at about 200 m above cloud base (1,200 m). This distribution is clearly bimodal and corresponds to the classical observations of total water distribution q_t for cumulus clouds (Lewellen and Yoh 1993; Neggers et al. 2007; Bogenschutz et al. 2010).

Thanks to the sampling, it is possible to isolate the distribution of s within the thermal (Fig. 1a) from that of the environment (Fig. 1b) and to show that the bi-modal nature of the distribution is associated with the organized structures (thermals). The s distribution

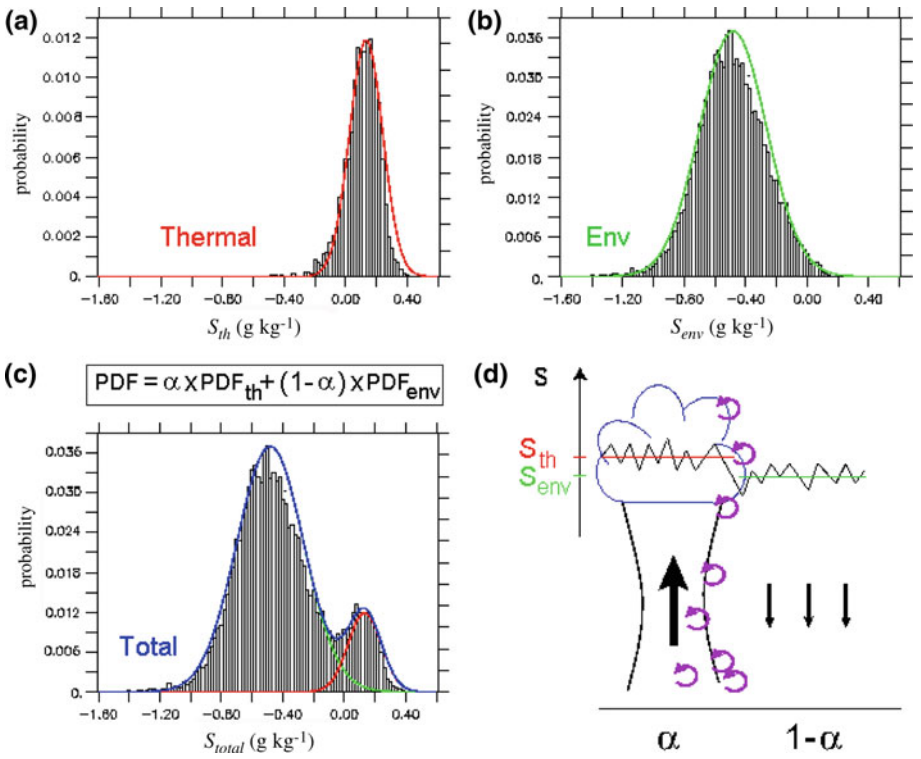

Fig. 1 Distributions of the saturation deficit s in (**a**) thermals, (**b**) environment and (**c**) the whole domain at 1,200 m for ARM hour 8. *Histograms* correspond to the conditional sampling results and the lines to the fit with Gaussian function in (**a**, **b**) and the total bi-Gaussian fit in (**c**). Frame (**d**) is a schematic view of the plume model with associated variations of s within cloud and the environment

is compared in Fig. 1c with the weighted average of two Gaussian distributions computed independently within the thermals (subscript 'th') and in their environment (subscript 'env'):

$$PDF(s) = (1-\alpha)\, f(s, \overline{s}_{\mathrm{env}}, \sigma_{\mathrm{env}}) + \alpha\, f(s, \overline{s}_{\mathrm{th}}, \sigma_{\mathrm{th}}) \tag{5}$$

with

$$f(s, \overline{s}, \sigma_{\mathrm{s}}) = \frac{1}{\sigma_{\mathrm{s}}\sqrt{2\pi}} \exp(-(s-\overline{s})^2/2{\sigma_{\mathrm{s}}}^2), \tag{6}$$

where $\overline{s}$ is the mean value of s, σ_{s} is its standard deviation and α is the fraction of grid points selected by the conditional sampling. Parameters $\overline{s}_{\mathrm{env}}$, σ_{env}, $\overline{s}_{\mathrm{th}}$, σ_{th} and α are here deduced directly from the LES conditional sampling. The two individual Gaussian distributions associated with the thermals and the environment are also superimposed on the sampled distribution in Fig. 1a, b. The bi-modal distribution is thus the combination of two uni-modal distributions associated with the thermals and their environment, which are satisfactorily approximated by Gaussian functions. This remains true for the entire boundary layer, both in the cloud and sub-cloud layers, except in the surface layer where the distribution of s is strongly negatively skewed.

2.4 Coupling the Bi-Gaussian Statistical Scheme with a Mass-Flux Representation of Boundary-Layer Thermals

We show here how the bi-Gaussian distribution can be coupled with any mass-flux scheme in which subgrid-scale variables are described through top-hat distributions. The bi-Gaussian distribution depends on five parameters: α, $\sigma_{s,env}$, $\sigma_{s,th}$, $\overline{s}_{env}$ and $\overline{s}_{th}$. Three of them are given directly by the mass-flux scheme: $\overline{s}_{env}$ and $\overline{s}_{th}$, which are computed from the top-hat distribution of q_t and θ_l (Eqs. 3 and 4), and α, which is either a parameter or an internal variable of the scheme (Soares et al. 2004; Rio and Hourdin 2008; Neggers 2009).

For $\sigma_{s,env}$ and $\sigma_{s,th}$, we propose simple relations based on the following general considerations. Whatever their shape or organization, thermal plumes consist of air parcels that rise from the surface, where the air properties are relatively well mixed. In the absence of lateral entrainment, internal mixing inside an individual thermal plume contributes to narrowing the in-thermal distribution. At the opposite, lateral mixing with the surrounding air, the properties of which significantly depart from the in-thermal properties, contributes to enlarging the in-thermal distribution of transported scalars. This effect is expected to be particularly strong for water distribution in the cumulus layer, where plumes of moist air arising from the surface generally penetrate a relatively dry environment. The detrainment of near-surface moist air by thermal plumes is also expected to provide a major contribution to the standard deviation of s in the environment within the cloud layer.

In this simple picture, where the lateral exchanges (through entrainment and detrainment) along the thermal plumes are the main source of variability of s within thermals and their environment, both $\sigma_{s,th}$ and $\sigma_{s,env}$ are expected to scale with the contrast $\overline{s}_{th} - \overline{s}_{env}$. Such a dependency is confirmed by the decomposition of the total variance of s according to the sampling of thermal plume structures shown in Fig. 2, where the contribution of the intra-environment variability ($(1-\alpha)\sigma^2_{s,env}$, full line) to the total variance (σ^2_s, squares) appears to scale with the "structure contribution" computed from the top-hat variables ($\alpha(1-\alpha)(\overline{s}_{th} - \overline{s}_{env})^2$, dashed line).

In the same idealized view, the thinner the thermal plume, the stronger the effect of mixing on the in-thermal width of the s distribution ($\sigma_{s,th}$) for a given $\Delta s = \overline{s}_{th} - \overline{s}_{env}$ contrast. At the opposite, thermals with a low fractional coverage α only weakly affect the width of the intra-environment distribution ($\sigma_{s,env}$). Thus $\sigma_{s,th}$ (respectively $\sigma_{s,env}$) is expected to increase (respectively decrease) when α decreases. Note that, at this level of consideration, this argument is valid even with a distribution of thermals of different widths and velocities.

In order to infer some tractable and robust relations for the parametrization, we consider the simplified image of an ensemble of plumes of similar width and vertical velocity so that the mean thermal plume of the parametrization can be assimilated to each individual plume. The free parameters of the proposed relations are then tuned to fit the LES results so that, at the end, the parametrization in part accounts for the effect of intra-thermal variations, or non-stationarity.

Considering any individual thermal plume, let us introduce A, the horizontal area associated with this single thermal plume and its environment (i.e. the inverse of the surface number density of plumes, assumed to be constant here). The section of the individual plume is then αA and its radius is $R = \sqrt{\alpha A/\pi}$ if assumed circular. For a layer of thickness δz, the area of the lateral exchange surface between the thermal and the environment is $\Sigma_l = 2\pi R \delta z$ while the volume inside the cylinder is $V_{th} = \alpha A \delta z$. In view of a control by lateral mixing, for a given value of the humidity contrast between the plume and the environment Δs, $\sigma_{s,th}$ is expected to scale with the ratio of the lateral mixing surface to the volume of the plume, $\Sigma_l/V_{th} = \sqrt{4\pi/A}/\sqrt{\alpha}$ while $\sigma_{s,env}$ scales with the ratio

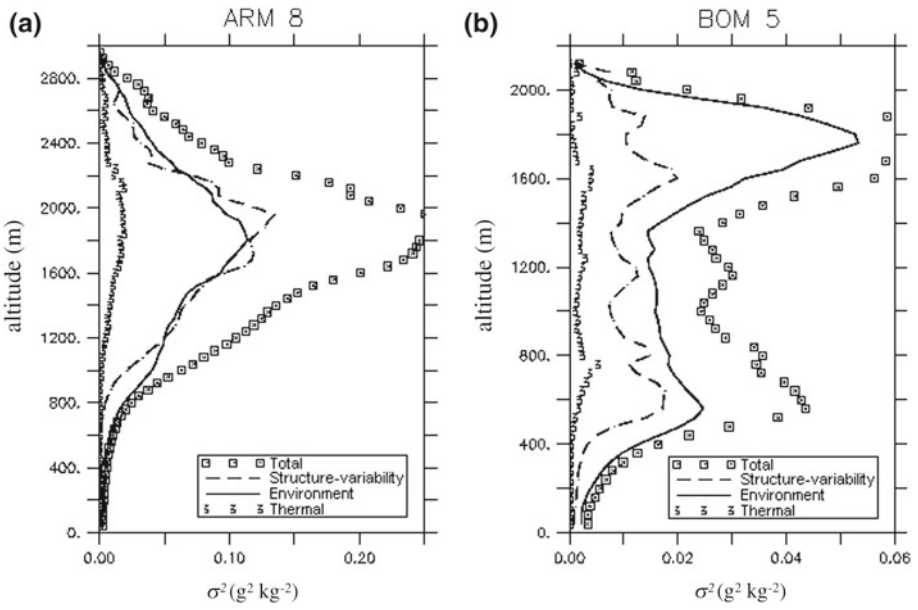

Fig. 2 Vertical profiles of contribution to variance of the conditional sampling structures ($\alpha(1-\alpha)(\overline{s}_{\rm th}-\overline{s}_{\rm env})^2$, *dashed line*), environment ($((1-\alpha)\sigma^2_{\rm s,env}$, *full line*), in-thermal ($\alpha\sigma^2_{\rm s,th}$, number 3) and the total variance ($\sigma^2_{\rm s}=\alpha(1-\alpha)(\overline{s}_{\rm th}-\overline{s}_{\rm env})^2+(1-\alpha)\sigma^2_{\rm s,env}+\alpha\sigma^2_{\rm s,th}$, *squares*) for ARM hour 8 and BOMEX hour 5

of Σ_1 to the volume $V_{\rm env} = A\,(1-\alpha)\,\delta z$ occupied by the environment of the plume, $\Sigma_1/V_{\rm env} = \sqrt{4\pi/A}\,\sqrt{\alpha}/(1-\alpha)$.

Finally, we have

$$\sigma_{\rm s,th} = c_{\rm th}\,\alpha^{-\frac{1}{2}}\,(\overline{s}_{\rm th}-\overline{s}_{\rm env}) + b\,\overline{q}_{t_{\rm th}} \tag{7}$$

and

$$\sigma_{\rm s,env} = c_{\rm env}\,\frac{\alpha^{\frac{1}{2}}}{1-\alpha}\,(\overline{s}_{\rm th}-\overline{s}_{\rm env}) + b\,\overline{q}_{t_{\rm env}}, \tag{8}$$

where $c_{\rm env}$ and $c_{\rm th}$ are tunable parameters, and the last term, $b\,\overline{q_{\rm t}}$, is an asymptotic value introduced for a value of $\alpha \approx 0$. This term is mostly important near the surface, where other processes such as turbulence or dry-air intrusion from the free troposphere contribute to the standard deviation. The PDF is then equivalent to a simple Gaussian distribution whose standard deviation σ is proportional to the mean total specific humidity $\overline{q}_{\rm t}$ (and not proportional to $\overline{s}$, as $\overline{s}$ could be close to zero or negative). Note that the particular power laws in α in the formulations depend partly on the simplified derivation made above. It is possible that a better fit could be reached with different power laws and a different set of tunable parameters, but a larger number of large-eddy simulations with appropriate sampling would probably be needed to discriminate between the different possible combinations.

The values of $b = 2\times10^{-3}$, $c_{\rm env} = 0.92$ and $c_{\rm th} = 0.09$ were chosen using LES results to obtain a good amplitude for the variations of $\sigma_{\rm s}$. It is noteworthy that $c_{\rm env}$ is about ten times larger than $c_{\rm th}$, which may in part reflect the oversimplification of the above derivation. In particular, only the dependency of the mixing to the s contrast and α was discussed in the above derivation of $\sigma_{\rm s,env}$ and $\sigma_{\rm s,th}$. The width of the distribution comes in fact from

a balance between lateral mixing that enlarges the distribution, and vertical advection that brings homogeneous air from the surface layer. The advection scales with the mean vertical velocity w within the thermal and within the environment. The advection is typically 10 times larger within the thermals since $\frac{w_{\text{th}}}{w_{\text{env}}} = \frac{1-\alpha}{\alpha}$ is typically $\sim$10. So the same mixing is 10 times more effective for the environment than for the plumes. This additional w dependency of $\sigma_{s,\text{env}}$ and $\sigma_{s,\text{th}}$, which could explain the ratio of the c_{env} and c_{th} coefficients, was not retained here for the sake of simplicity but could deserve further investigation.

Recent studies (Heus and Jonker 2008) have also shown that the environmental subsidence occurs partly in narrow shells surrounding the cumulus clouds, in both observations and LES. The concentration of subsidence into shells in the environment might also be an explanation for this greater variance of s within the environment than within the thermals.

Note that our parametrization presents some similarities with that proposed by Neggers (2009). In Neggers (2009), the equivalent of σ_{th} also increases with the difference of two mean total specific humidities, $\overline{q}_{\text{t,test}} - \overline{q}_{\text{t,th}}$, where $\overline{q}_{\text{t,test}}$ is the total specific humidity of a test parcel initialized with the properties of the 0.002 upper fraction of the distribution of q, and $\overline{q}_{\text{t,th}}$ is the mean total specific humidity within the moist updraft. σ_{th} also varies with the fractional area a_{u2} occupied by the moist updraft. However, σ_{env} is then deduced from a budget equation of the total variance σ_{t} and from the value of σ_{th} while it is parametrized in the same way as is σ_{th} in our scheme.

Our parametrization for the widths of the distribution, even though based on simple physical considerations, enables us to reproduce the time and height variability of the in-thermal and environment distributions in the BOMEX and ARM cases as shown below.

2.5 Evaluation of the Standard Deviation Formulations in the LES

The skill of the formulations proposed for the computation of the standard deviations of the saturation deficit PDF is first illustrated in Fig. 3 for hour 8 of the ARM case by comparing the PDFs issued from the LES with the bi-Gaussian scheme. The bi-Gaussian function captures reasonably well the various shapes obtained in the LES, both below and within the cloud layer. While the standard deviations of the individual Gaussian were computed directly from the sampled distributions in Fig. 1, only $\overline{s}_{\text{th}}$, $\overline{s}_{\text{env}}$ and α are computed here from the conditional sampling of the LES, σ_{th} and σ_{env} being computed thanks to Eq. 7 and Eq. 8 respectively.

In order to illustrate further the ability of the new parametrization to compute the moments of the distribution of s, we concentrate on hour 8 of the ARM simulation (1330 LT) that corresponds to developed shallow convection, and hour 5 of BOMEX. The values of $\sigma_{s,\text{env}}$ (Fig. 4a, b) and $\sigma_{s,\text{th}}$ (Fig. 4c, d) derived from the sampled distributions, as well as the total standard deviation $\sigma_{s,\text{total}}$ (Fig. 4e, f) and skewness (Fig. 4g, h) over the full domain computed directly from the LES results, are compared with their estimation from the parametrized bi-Gaussian distribution using the sampled values of α, $\overline{s}_{\text{env}}$ and $\overline{s}_{\text{th}}$ in LES. In general, the proposed formulations capture the vertical evolution of both standard deviations $\sigma_{s,\text{env}}$ and $\sigma_{s,\text{th}}$ as well as the total standard deviation and skewness. Comparison with values computed with a constant value of $\alpha = 0.1$ (in blue, dashed line) illustrates the importance of taking into account the dependency on α, especially for $\sigma_{s,\text{env}}$.

In the upper part of the cloud layer, Eq. 8 tends to underestimate $\sigma_{s,\text{env}}$ both for ARM and BOMEX, whereas Eq. 7 overestimates $\sigma_{s,\text{th}}$. This occurs for heights >2,200 m for ARM and 1,600 m for BOMEX. In this region of the cloud layer, α is $< 1\,\%$, so that the conditional sampling is not very accurate for statistical reasons. Since in the formulations, $\sigma_{s,\text{env}}$ varies as $\alpha^{\frac{1}{2}}$ and $\sigma_{s,\text{th}}$ as $\alpha^{-\frac{1}{2}}$, the fact that $\sigma_{s,\text{env}}$ is too small and $\sigma_{s,\text{th}}$ too large could be due to

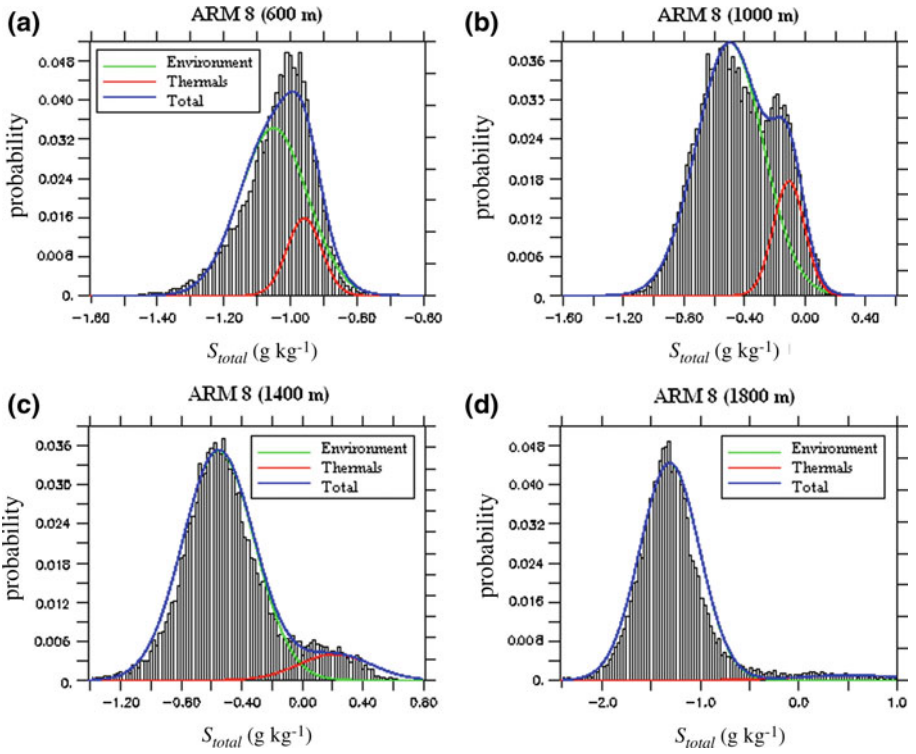

Fig. 3 Distributions of s for the ARM case hour 8. The *histograms* (*bars*) correspond to the LES distributions at various heights: (**a**) 600 m, (**b**) 1,000 m, (**c**) 1,400 m and (**d**) 1,800 m. The Gaussian distributions within the environment (*green*), within the thermals (*red*) as well as the combined bi-Gaussian distribution (*blue*) are superimposed. The tracer based conditional sampling is used to compute the values of $\overline{s}_{\text{th}}$, $\overline{s}_{\text{env}}$ and α from the LES while σ_{th} and σ_{env} are computed thanks to Eqs. 7 and 8 respectively

an underestimation in α. The vertical profile of the skewness (Fig. 4g, h) is also reproduced by the bi-Gaussian distribution except in the surface layer where intrusions of dry air from the free troposphere (dry tongues, Couvreux et al. 2007), which are not taken into account, involve a negative skewness.

The agreement with LES is not restricted to the two particular hours retained for illustration. The scatter plots between the LES and parametrized estimations of $\sigma_{\text{s,env}}$, $\sigma_{\text{s,th}}$, $\sigma_{\text{s,total}}$ and skewness (Fig. 5) show that the parametrization is valid throughout the simulation, for both the ARM and BOMEX cases, and for all altitudes, both below and within the cloud layer.

2.6 Computation of Cloud Properties

Once the PDF is known, it becomes possible to compute the cloud fraction

$$c = \int_0^{\infty} f(s)\, ds \tag{9}$$

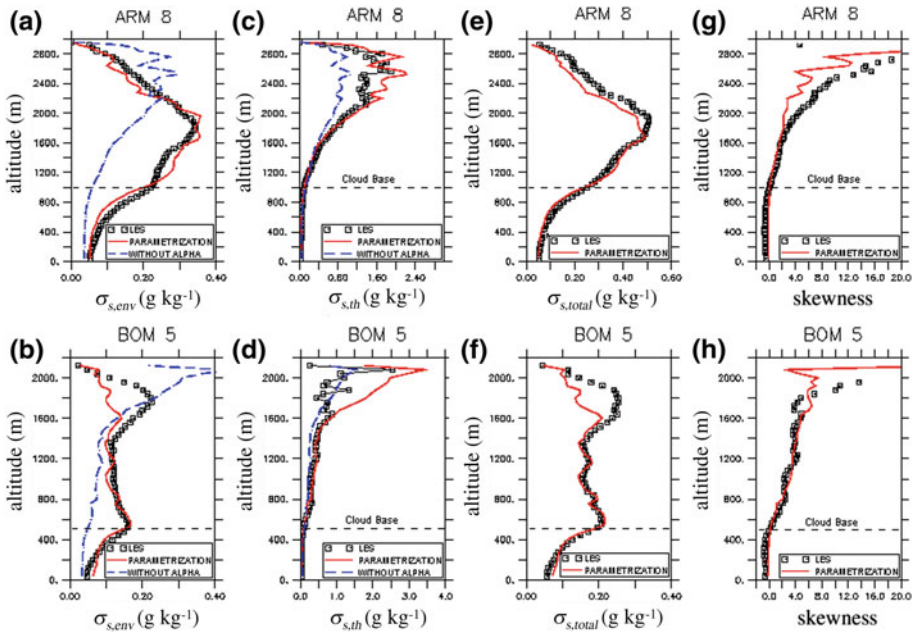

Fig. 4 Vertical profiles of the standard deviation of s in the environment ($\sigma_{s,env}$), Frames (**a**) and (**b**), in the thermals ($\sigma_{s,th}$, Frames (**c**) and (**d**), in the whole domain ($\sigma_{s,total}$, Frames (**e**) and (**f**) and of skewness (Frames (**g**) and (**h**)) derived from LES (*squares*), or using the bi-Gaussian formulation (*red curves*) respectively for the ARM case hour 8 and for the BOMEX case hour 5 of simulation. For $\sigma_{s,env}$ and $\sigma_{s,th}$, the *blue curves* correspond to estimations using a constant value for $\alpha = 0.1$ in place of the value given by the sampling and with a variable (*red curves*)

and liquid water content

$$q_c = \int_0^\infty s\, f(s)\, ds. \tag{10}$$

In Fig. 6, we compare the cloud fraction c and liquid water q_c obtained with a bi-Gaussian PDF (red line), with a single Gaussian PDF (black full line), with a log-normal PDF (black dashed line) and that computed directly from LES (squares).

To compute c and q_c with the bi-Gaussian distribution derived above, variables $\overline{s}_{th}$, $\overline{s}_{env}$ and α are computed using the conditional sampling, and standard deviations σ_{env} and σ_{th} are calculated using Eqs. 7 and 8. For the single Gaussian scheme, the PDF of the saturation deficit s is a single Gaussian function centered on $\overline{s}$. This scheme requires only two parameters, $\overline{s}$ and its standard deviation σ_s, which are taken directly from LES for the figure.

For the log-normal distribution, the PDF of q_t is a log-normal function bounded by zero and centered on $\overline{q_t}$ used presently as the cloud scheme in LMDZ. This scheme, developed by Bony and Emanuel (2001), requires two input variables, the in-cloud water content $\overline{q}_{c,in}$ and $\overline{q}_t$, which are taken directly from LES for the figure. Analytical expressions of c and q_c for each scheme are given in the Appendix.

With the single Gaussian PDF, the cloud fraction is underestimated at all heights and for both cases (except in the ARM case between 1,200 and 1,400 m). This is especially noteworthy in the BOMEX case where the cloud fraction becomes null over 1,000 m whereas it should

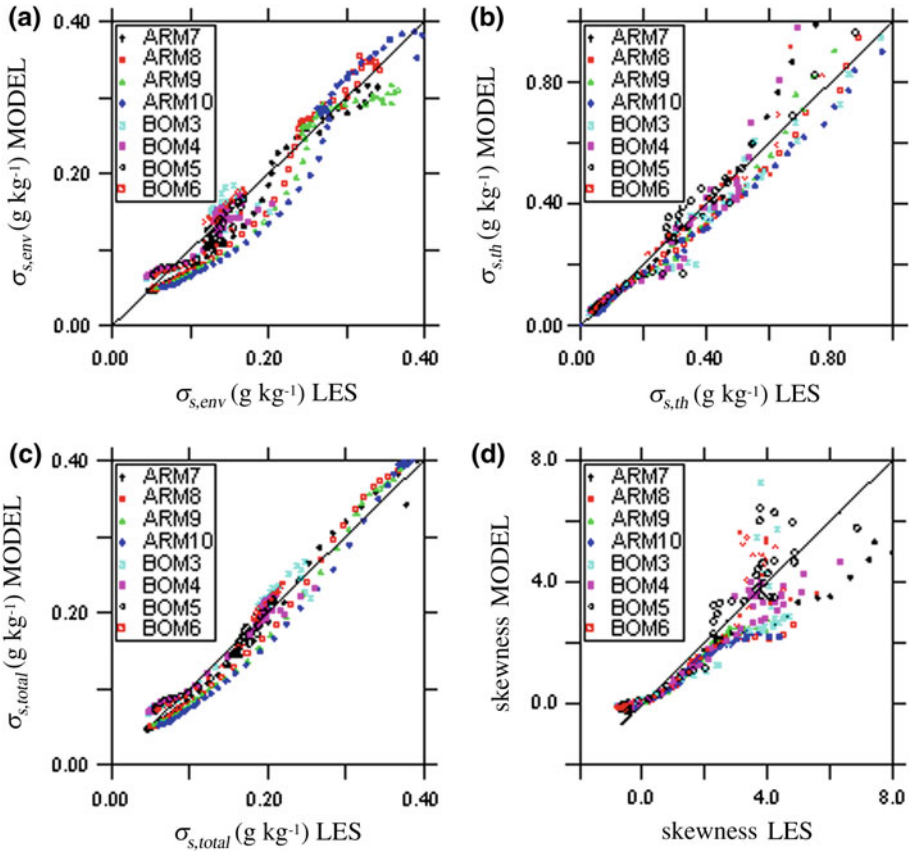

Fig. 5 Scatter plots of standard deviations (**a**) $\sigma_{s,env}$, (**b**) $\sigma_{s,th}$, (**c**) $\sigma_{s,total}$ and (**d**) skewness computed from LES versus parametrized values for the BOMEX case, hours 3, 4, 5 and 6, and for the ARM case, hours 7, 8, 9 and 10. Each *point* represents an hour and a vertical level

be about 2 % up to 1,600 m and should decrease to zero towards 2,000 m. The condensed water variable q_c is also widely underestimated for both cases and at all heights, especially in the upper part of the clouds. To understand this behaviour, it is necessary to report the distribution of the saturation deficit s at 1330 LT (hour 8) for the ARM case, at 1,200 m (Fig. 7b). The extreme right part of the Gaussian PDF generally exceeds the maximum value of s, and therefore the cloud base is slightly lower than that given by LES. In the rest of the cloud, the Gaussian PDF fails at reproducing the second mode of the s distribution, and the condensed water q_c is too small.

With the log-normal cloud scheme, condensed water is an input variable of the scheme. In practice, $q_{c,in}$ is used to compute a factor k from an inverse procedure from which the cloud fraction c and the condensed water q_c are computed (see Appendix).[1] With this scheme, cloud base is located satisfactorily well, but the cloud fraction c increases too slowly and the maximum is located at a level higher than expected (1,400 m for ARM instead of 1,100 and

[1] The computed condensed water q_c is not exactly superimposed on the LES results as should be the case, due to numerical instabilities in the computation of k in the inverse procedure.

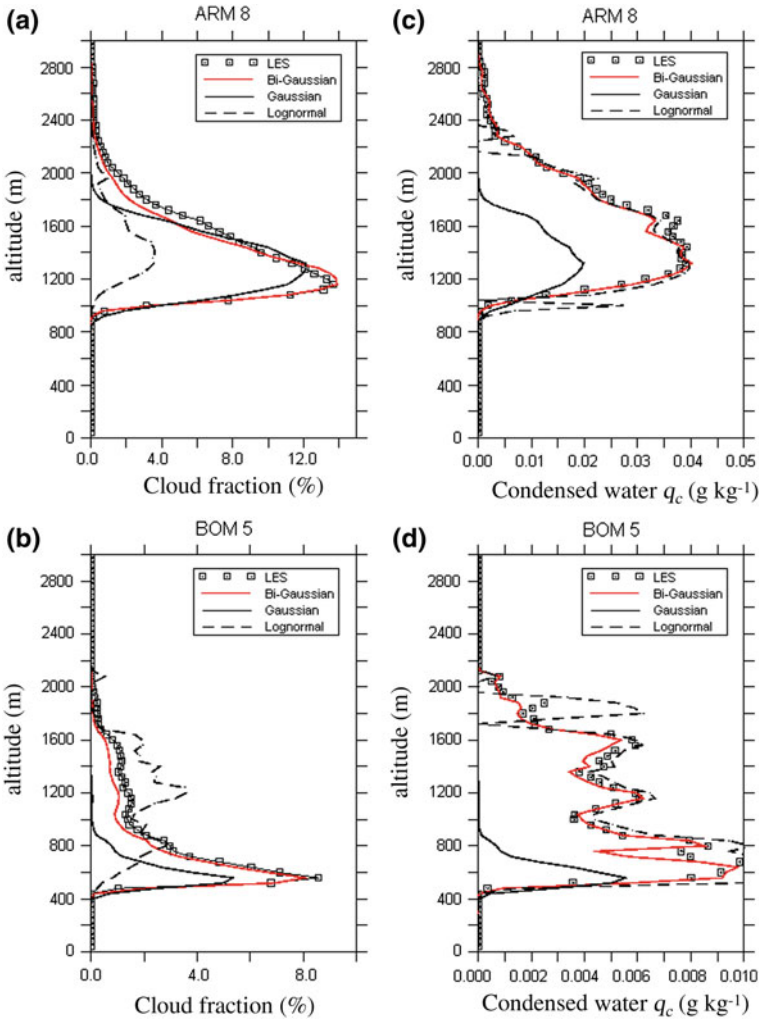

Fig. 6 Vertical profiles of cloud fraction c and condensed water q_c in LES (*squares*), derived from the bi-Gaussian distribution of s scheme (*red*), from a single Gaussian distribution scheme (*black full line*) and from the q_t Bony-Emanuel log-normal PDF scheme (*dashed*)

800 m in BOMEX instead of 550 m). The cloud fraction is too small, especially for ARM, but is satisfactory in the upper part of the cloud layer.

Figure 7a illustrates how the proposed bi-Gaussian PDF reproduces the distribution of total specific humidity q_t or saturation deficit s for shallow cumulus convection cases. Compared with the Gaussian and log-normal distributions, it allows us to fit better the right part of the distribution, corresponding to values of $q_t >$ the saturation q_{sat}. Finally, as expected and discussed previously (Lewellen and Yoh 1993; Larson 2002; Perraud et al. 2011), using a bi-Gaussian PDF of the saturation deficit s leads to a satisfactory representation of clouds except for the amplitude of the cloud fraction that is slightly underestimated in the upper part of the cloud layer. In particular, the position of the maximum cloud fraction is in better agreement with LES results than with the log-normal PDF used previously in the LMDZ model.

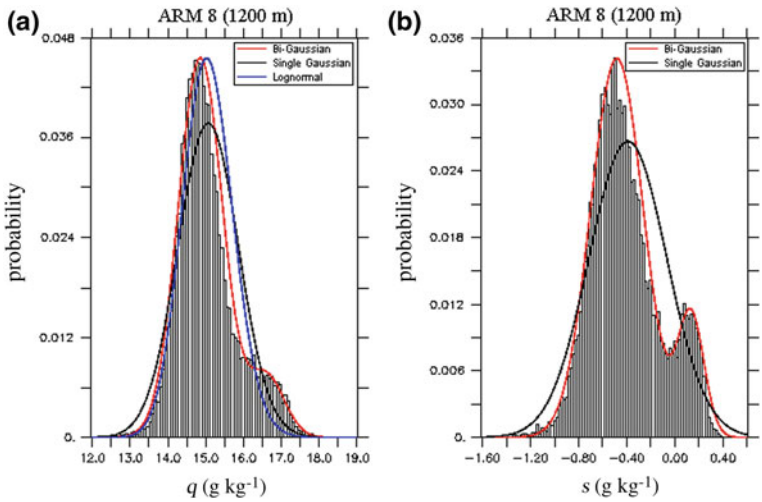

Fig. 7 Distribution of (**a**) total water content q and (**b**) saturation deficit s for ARM hour 8 at 1,200 m. The single Gaussian PDF (*black*), the Bony-Emanuel log-normal PDF (*blue*) and the bi-Gaussian PDF (in *red*) are superimposed

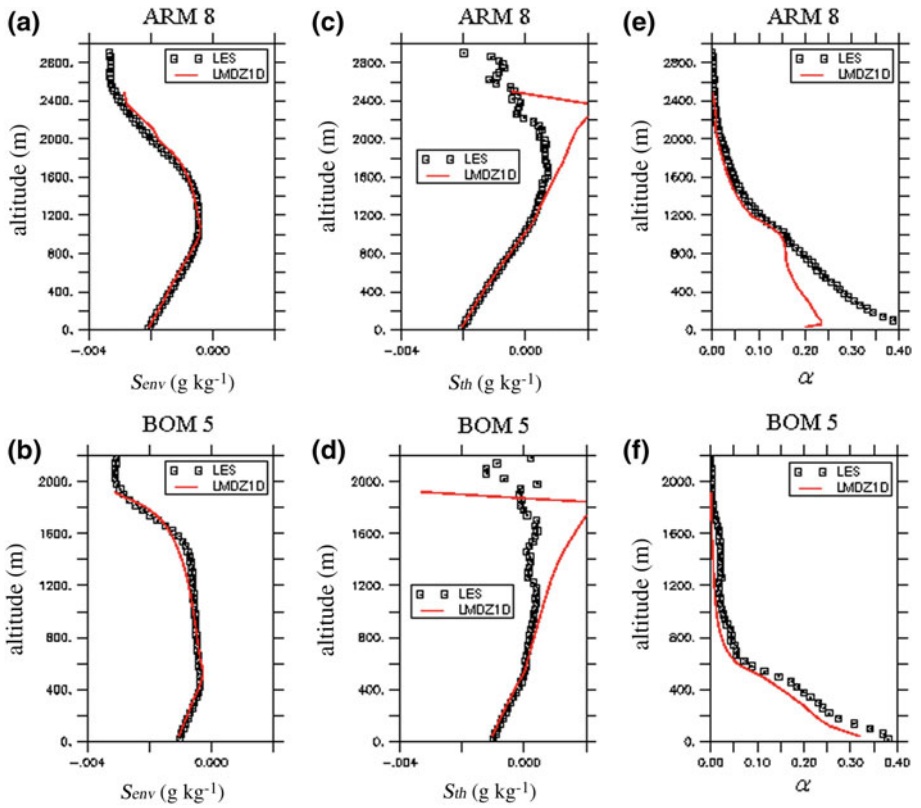

Fig. 8 Vertical profiles of $\overline{s}_{\mathrm{env}}$, $\overline{s}_{\mathrm{th}}$ and thermal fraction α computed with the LMDZ1D model (*red*) and derived from the LES sampling (*squares*) for ARM (hour 8) and BOMEX (hour 5)

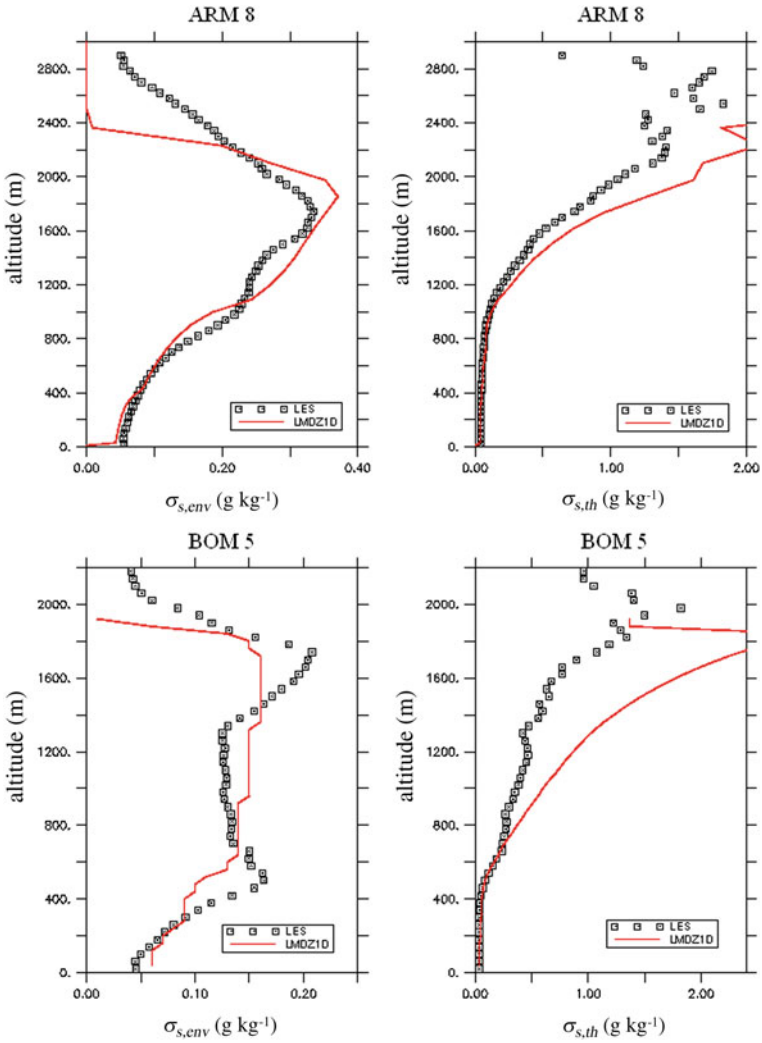

Fig. 9 Vertical profiles of σ_{env} and σ_{th} computed with the LMDZ1D model (*red*) and derived from the conditional sampling (*squares*) for ARM hour 8 and BOMEX hour 5

An important point to note here is that the bi-Gaussian is not a fit of the LES distribution but instead uses the estimations of $\sigma_{\text{s,env}}$ and $\sigma_{\text{s,th}}$ given by Eqs. 7 and 8, and thus relies only on the values of α, $\overline{s}_{\text{th}}$ and $\overline{s}_{\text{env}}$ sampled in the LES.

3 Test in a Single Column Model

3.1 The Single Column Version of LMDZ

Simulations are made using the most recent version LMDZ5 of the global climate model of Laboratoire de M*ét*éorologie Dynamique (Hourdin et al. 2012), involved in particular in the

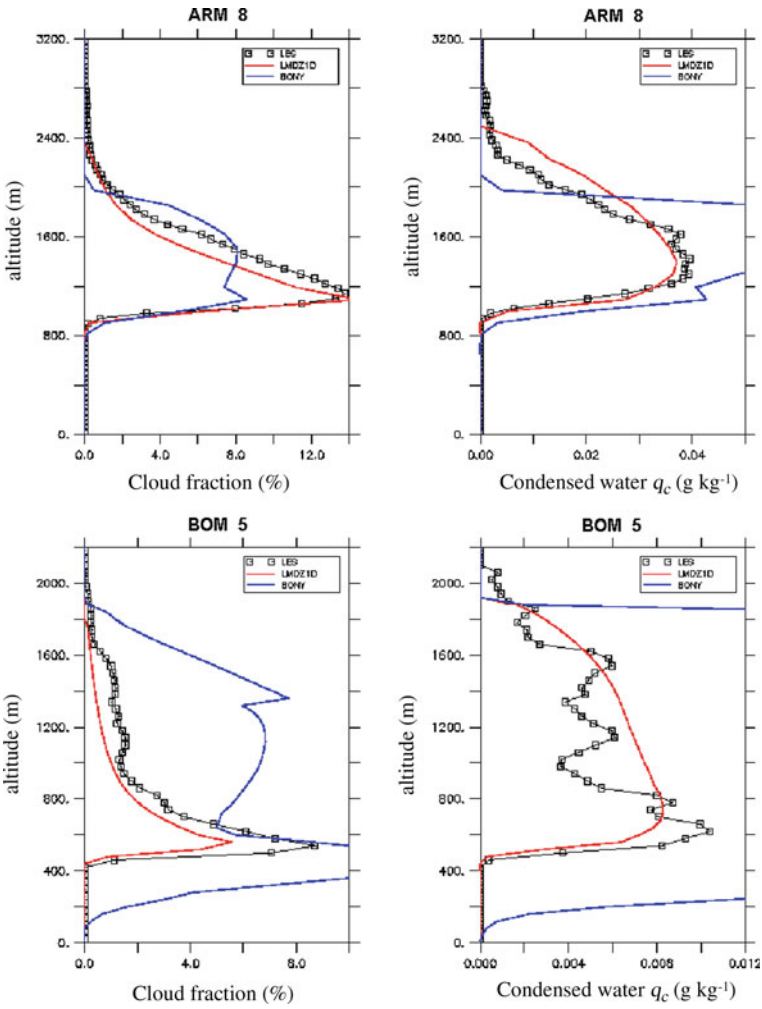

Fig. 10 Vertical profiles of cloud fraction c and condensed water q_c computed with LMDZ1D bi-Gaussian cloud Scheme (*red*) and LMDZ1D Bony-Emanuel cloud scheme (*blue*) compared with LES (*squares*) for ARM hour 8 and BOMEX hour 5

CMIP program that coordinates the climate change experiments for the assessment reports of the Intergovernmental Panel on Climate Change (IPCC) (Dufresne et al. 2005).

The boundary-layer representation includes a parametrization of eddy diffusion based on a prognostic equation for the turbulent kinetic energy (Yamada 1983) as well as the thermal plume model (Rio and Hourdin 2008) for shallow convection. We use here the fractional detrainment rate δ and entrainment rate ϵ described in Rio et al. (2010). For the cloud, we run either the log-normal scheme of Bony and Emanuel (2001) or the new bi-Gaussian scheme.

The ARM case is run with a vertical resolution of 40 levels and a timestep of 60 s, while the BOMEX case is run with a finer vertical grid of 100 levels in order to have approximately the same number of levels in the cloudy part as for the ARM case, and a timestep of 60 s. Output variables are 10-min averaged.

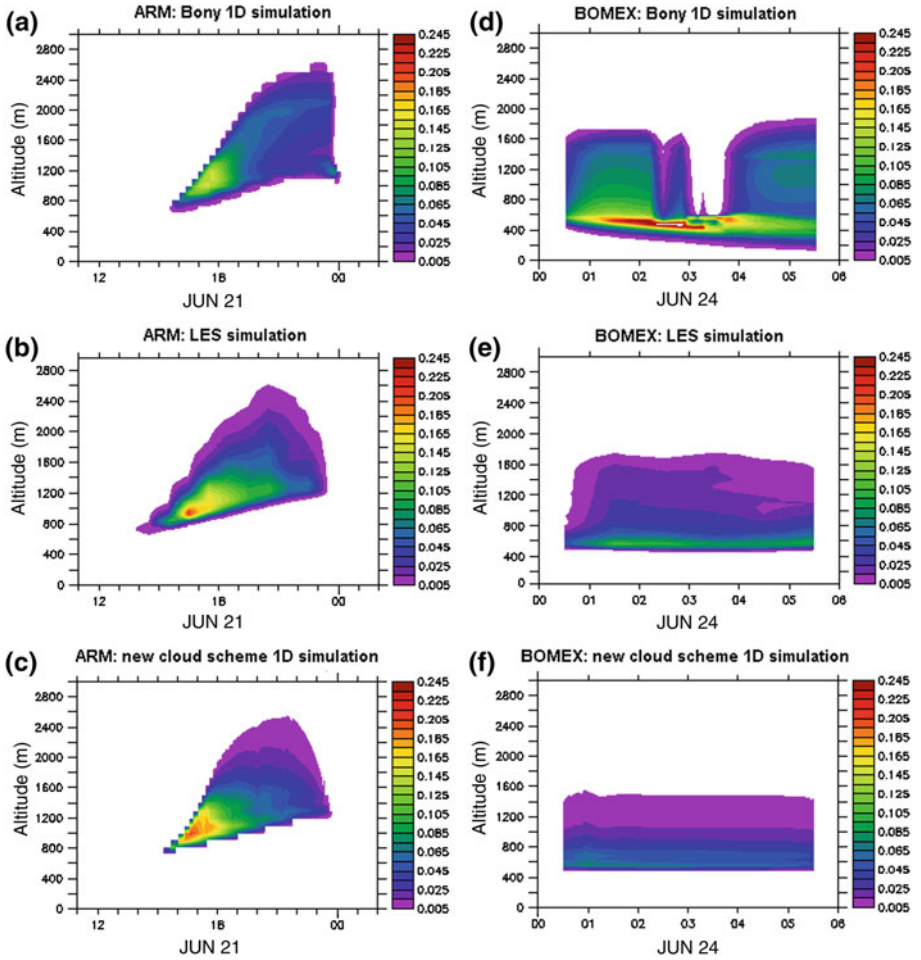

Fig. 11 Comparison between cloud fraction computed with LMDZ1D log-normal cloud scheme for ARM (**a**) and BOMEX (**d**), cloud fraction given by LES for ARM (**b**) and BOMEX (**e**), and cloud fraction computed with LMZD1D bi-Gaussian cloud scheme for ARM (**c**) and BOMEX (**f**)

3.2 Simulation of the s Distribution

In the single column simulations, the meteorological state variables as well as the internal variables of the parametrizations evolve from an initial state, according to the model equations. The skill of the new cloud scheme then relies on the ability of the thermal plume model to accurately predict the values of α, $\overline{s}_{\text{env}}$ and $\overline{s}_{\text{th}}$. These values of s are directly computed from the "top hat" values of $\overline{q}_t$, $\overline{\theta}_{\text{l}}$ and $\overline{q}_{\text{sat}}$ given by the thermal plume model (Rio and Hourdin 2008); α is also computed by the thermal plume model.

Figure 8 shows $\overline{s}_{\text{env}}$, $\overline{s}_{\text{th}}$ and α computed with LMDZ1D and compared with LES for the ARM case (hour 8) and for the BOMEX case (hour 5). The cloud layer is located between 1,000 and 2,500 m for ARM, and between 400 and 2,000 m for BOMEX, so that we focus our interest between these heights. Variable α is well reproduced in LMDZ1D within the cloud layer for the ARM case (Fig. 8e) and slightly underestimated for all heights in BOMEX

(Fig. 8f). In both cases, α decreases from cloud base (about 15 %) to cloud top (zero), illustrating the importance for α as a variable in the mass-flux scheme. The saturation deficit within the environment $\overline{s}_{\rm env}$ is consistent with LES data for both simulations at all heights (Fig. 8a, b); the saturation deficit within thermals, $\overline{s}_{\rm th}$, is well represented up to 1,800 m for the ARM case (Fig. 8c) and 1,200 m for BOMEX (Fig. 8d), but too large above. It seems to be a significant bias of the thermal plume model that the upper part of the cloud layer is too moist.

The standard deviations $\sigma_{\rm s,env}$ and $\sigma_{\rm s,th}$ obtained in the single column simulations are compared to the sampled LES values in Fig. 9; $\sigma_{\rm s,th}$ is well reproduced below 1,600 m for ARM and 1,000 m for BOMEX (Fig. 9c, d). Above these heights, the saturation deficit $\overline{s}_{\rm th}$ is overestimated and so is the difference $\overline{s}_{\rm th} - \overline{s}_{\rm env}$, which induces an overestimation of the parametrized $\sigma_{\rm s,th}$ and $\sigma_{\rm s,env}$. Note that the errors on the s and $\sigma_{\rm s}$ profiles above 1,800 m for ARM and 1,200 m for BOMEX compensate and lead to a better agreement for x variables, $x_{\rm env} = -\overline{s}_{\rm env}/\sigma_{\rm s,env}$ and $x_{\rm th} = -\overline{s}_{\rm th}/\sigma_{\rm s,th}$, variables used for the computation of cloud fraction c and condensed water $q_{\rm c}$ (see the Appendix). Generally, profiles of x are in good agreement with those issued from LES (not shown).

3.3 Simulation of Cloud Properties

Figure 10 shows the vertical profiles of $q_{\rm c}$ and c as simulated with LMDZ1D using either the new cloud scheme (red continuous line) or the Bony-Emanuel log-normal cloud scheme (blue continuous line), compared with LES results (squares) at hour 8 of ARM and hour 5 of BOMEX. As expected, cloud fractions for both cases are well reproduced where parameters α and x are well represented. Especially, comparing with the Bony log-normal cloud scheme, cloud base and the maximum of cloud fraction are better localized. The thickness of the cloud, as well as the vertical decrease of the cloud fraction is also well simulated. Condensed water $q_{\rm c}$ is also in good agreement with LES data even though slightly overestimated in the upper part of clouds. This is mainly due to the overestimation of $\sigma_{\rm s}$. Figure 11 finally shows, for the same two schemes and for the LES, the time evolution of the cloud fraction for ARM and BOMEX in order to illustrate that the better behaviour of the new bi-Gaussian statistical cloud scheme is observed throughout these two simulations.

4 Conclusions

The following main outcomes can be drawn from this study:

1. The bi-modal nature of the saturation deficit for the convective boundary layer within and below clouds is confirmed.
2. The potential offered by the tracer-based conditional sampling that isolates the coherent structures of the boundary layer and enables a thorough evaluation of parametrizations is highlighted. The conditional sampling allows us in particular to attribute one mode to plumes of buoyant air arising from the surface and the other to the environment. This situation prevails except in the lower part of the sub-cloud layer where dry tongues of air coming from the free troposphere also play a significant role (Couvreux et al. 2007).
3. A new statistical cloud scheme based on a bi-Gaussian distribution of s is proposed. Each Gaussian distribution is centered on the mean of s within the thermal plume and its mean in the environment. The width of the s distribution is assumed to depend on the exchange efficiency between plumes and the environment. This leads to expressions for $\sigma_{\rm s,env}$ and $\sigma_{\rm s,th}$ that scale with the humidity contrast $\overline{s}_{\rm th} - \overline{s}_{\rm th}$, $\sigma_{\rm s,env}$ increasing while

$\sigma_{s,th}$ decreases with increasing values of α. Those expressions are tuned and evaluated against LES results.

4. Thanks to the formulations of $\sigma_{s,env}$ and $\sigma_{s,th}$, the bi-Gaussian can be coupled with any mass-flux scheme that provides separately the mean thermodynamical air properties in the updrafts and in their environment, as well as the fractional coverage of the updrafts.
5. Combined with the thermal plume model of Rio and Hourdin (2008), the new statistical cloud scheme leads to a reasonable representation of both cloud cover and liquid water content in single column simulations of the marine and continental convective boundary layer.

Some aspects of this study deserve further investigation and refinements. First, the tracer-based conditional sampling has been modified for this study, but the choices made on the thresholds and combinations of variables are still quite arbitrary and not totally satisfactory. A strategy could be pursued to try to build a sampling on the unique use of one or maybe two tracers, in order to avoid interference of sampling criteria with the processes considered (the use of condensed water in the sampling, for instance, is in particular non neutral when defining cloud related properties).

The particular power laws retained for the α dependency of $\sigma_{s,env}$ and $\sigma_{s,th}$ may depend in part on the choice made on the geometry and organization of thermals in the derivation. This particular choice leads to relations that are compatible with the LES results; however it is possible that a somewhat different combination of power laws and tunable parameters could lead to similar or even better fits of the LES results. Also the fact that the tunable parameters c_{th} and c_{env} differ by an order of magnitude may indicate that other dependencies should be accounted for, and probably here the dependency on the vertical velocity w of the thermal plumes. This additional complexity has not been considered so far in the LMDZ model.

Another important aspect is the extension of the new statistical cloud scheme to other conditions, and in particular to stratocumulus conditions that were not considered here, and are known to be particularly important for climate models but difficult to parametrize. This requires further developments in the parametrization of entrainment and detrainment within thermal plumes that are underway. Also further investigations should be made on the potential role and parametrization of the negative skewness of the PDF of saturation deficit s in the lower part of the boundary layer, associated with dry tongues originating from the free troposphere.

The parametrization presented in this study, coupled to the thermal plume model, is already implemented in a new version of the LMDZ general circulation model (LMDZ5B). Compared to the previous LMDZ5A version, the representation of shallow cumulus clouds was significantly improved, in particular in the region of the trade winds.

4.1 Appendix

From the knowledge of the s probability distribution function $f(s)$, cloud fraction c and liquid water q_c are computed, according to Eqs. 9 and 10. For a single Gaussian distribution, cloud fraction c_{sg} is given by

$$c_{sg}(x) = \frac{1}{2}(1 - \mathrm{erf}(x)) \tag{11}$$

where $x = -\bar{s}/\sigma_s$ and liquid water q_c is given by

$$q_{c,sg}(x) = \sigma_s \left[\frac{1}{\sqrt{2\pi}} \exp(-x^2) - \frac{x}{\sqrt{2}}(1 - \mathrm{erf}(x)) \right]. \tag{12}$$

For the bi-Gaussian distribution, the total cloud fraction c_{bg} and total liquid water $q_{\mathrm{c,bg}}$ are a linear combination of the calculated values for environment and thermal plume

$$c_{\mathrm{bg}} = (1-\alpha)\, c_{\mathrm{sg}}(x_{\mathrm{env}}) + \alpha\, c_{\mathrm{sg}}(x_{\mathrm{th}}), \tag{13}$$

and

$$q_{\mathrm{c,bg}} = (1-\alpha)\, q_{\mathrm{c,sg}}(x_{\mathrm{env}}) + \alpha\, q_{\mathrm{c,sg}}(x_{\mathrm{th}}), \tag{14}$$

where $x_{\mathrm{env}} = -\overline{s}_{\mathrm{env}}/\sigma_{\mathrm{s,env}}$ and $x_{\mathrm{th}} = -\overline{s}_{\mathrm{th}}/\sigma_{\mathrm{s,th}}$.

For the Bony and Emanuel (2001) scheme, based on a generalized log-normal bounded by zero, the probability distribution function (PDF) of total specific humidity q_{t}, q_{inc} is given by

$$q_{\mathrm{inc}} = \overline{q_{\mathrm{t}}} \left[\frac{1 - \mathrm{erf}\left(\frac{\delta}{k\sqrt{2}} + \frac{k}{2\sqrt{2}}\right)}{1 - \mathrm{erf}\left(\frac{\delta}{k\sqrt{2}} - \frac{k}{2\sqrt{2}}\right)} - e^{-\delta} \right] \tag{15}$$

where $\delta = \ln\left(\frac{\overline{q_{\mathrm{t}}}}{q_{\mathrm{sat}}}\right)$ and $k = -\sqrt{\ln[1 + (\frac{\sigma}{\overline{q_{\mathrm{t}}}})^2]}$.

Since in-cloud water content is predicted by the thermal plume model, it is possible, from an inverse procedure, to predict the value of k, and to compute the value of cloud fraction c given by

$$c_{ln} = \frac{1}{2}\left[1 - \mathrm{erf}\left(\frac{\delta}{k\sqrt{2}} - \frac{k}{2\sqrt{2}}\right)\right]. \tag{16}$$

References

Bechtold P, Cuijpers JWM, Mascart P, Trouilhet P (1995) Modeling of trade wind cumuli with a low-order turbulence model: toward a unified description of Cu and Sc clouds in meteorological models. J Atmos Sci 52:455–463

Bogenschutz PA, Krueger SK, Khairoutdinov M (2010) Assumed Probability Density Functions for shallow and deep convection. J Adv Model Earth Syst 42:Art. #10, 24 pp

Bony S, Emanuel KA (2001) A parametrization of cloudiness associated with cumulus convection; evaluation using Toga Coare data. J Atmos Sci 58:3158–3183

Bougeault P (1981) Modeling the trade-wind cumulus boundary layer. Part I: testing the ensemble cloud relations against numerical data. J Atmos Sci 38:2414–2428

Brown A, Cederwall R, Chlond A, Duynkerke P, Golaz J-C, Khairoutdinov M, Lewellen D, Lock A, Macvean M, Moeng C-H, Neggers R, Siebesma A, Stevens B (2002) Large-eddy simulation of the diurnal cycle of shallow cumulus convection over land. Q J R Meteorol Soc 128:1075–1093

Chaboureau JP, Bechtold P (2002) A simple cloud parametrization derived from cloud resolving model data: Diagnostic and prognostic applications. J Atmos Sci 59:2362–2372

Couvreux F, Guichard F, Redelsperger J-L, Flamant C, Masson V, Kiemle C, Lafore J-P (2005) Water vapour variability within a convective boundary layer assessed by large eddy simulations and IHOP observations. Q J R Meteorol Soc 131:2665–2693

Couvreux F, Guichard F, Masson V, Redelsperger J-L (2007) Negative water vapour skewness and dry tongues in the convective boundary layer: observations and large-eddy simulation budget analysis. Boundary-Layer Meteorol 123:269–294

Couvreux F, Hourdin F, Rio C (2010) Resolved versus parametrized boundary layer thermals. Part I: a parametrization oriented conditional sampling in large eddy simulations. Boundary-Layer Meteorol 134:441–458

Deardorff JW (1972) Theoretical expression for the countergradient vertical heat flux. J Geophys Res 77:5900–5904

Dufresne J-L, Quaas J, Boucher O, Denvil S, Fairhead L (2005) Contrasts in the effects on climate of anthropogenic sulfate aerosols between the 20th and the 21st century. Geophys Res Lett 32:L21703. doi:10.1029/2005GL0236619

Emanuel KA (1993) A cumulus representation based on the episodic mixing model: the importance of mixing and microphysics in predicting humidity. The representation of cumulus convection in numerical models of the atmosphere. Meteorological Monograph No. 46. American Meteorological Society, Boston, pp 185–192
Fouquart Y, Bonnel B (1980) Computations of solar heating of the Earth's atmosphere: a new parametrization. Contrib Atmos Phys 53:35–62
Golaz J-C, Larson VE, Cotton WR (2002a) A PDF-based model for boundary layer clouds. Part I: method and model description. J Atmos Sci 59:3540–3551
Golaz J-C, Larson VE, Cotton WR (2002b) A PDF-based model for boundary layer clouds. Part II: model results. J Atmos Sci 59:3552–3571
Heus T, Jonker HJJ (2008) Subsiding shells around shallow cumulus clouds. J Atmos Sci 65:1003–1018
Holland JZ, Rasmusson EM (1973) Measurement of atmospheric mass, energy and momentum budgets over 500-kilometer square of tropical ocean. Mon Weather Rev 101:44–55
Hourdin F, Couvreux F, Menut L (2002) Parameterisation of the dry convective boundary layer based on a mass flux representation of thermals. J Atmos Sci 59:1105–1123
Hourdin F, Musat I, Bony S, Braconnot P, Codron F, Dufresne J-L, Fairhead L, Filiberti M-A, Friedlingstein P, Grandpeix J-Y, Krinner G, LeVan P, Li Z-X, Lott F (2006) The LMDZ4 general circulation model: climate performance and sensitivity to parametrized physics with emphasis on tropical convection. Clim Dyn 27:787–813
Hourdin F, Grandpeix J-Y, Rio C, Bony S, Jam A, Cheruy F, Rochetin N, Fairhead L, Idelkadi A, Musat I, Dufresne J-L, Lefebvre M-P, Lahellec A, Roehrig R (2012) LMDZ5B: the atmospheric component of the IPSL climate model with revisited parametrizations for clouds and convection. Clim Dyn. doi:10.1007/s00382-012-1343-y
Lafore J-P, Stein J, Ascencio N, Bougeault P, Ducrocq V, Duron J, Fisher C, Mascart P, Masson V, Pinty J-P, Redelsperger J-L, Richard E (1998) The meso-nh atmospheric simulation system. Part I: adiabatic formulation and control simulations. Ann Geophys 16:90–109
Larson VE (2002) Small-scale and mesoscale variability in cloudy boundary layers: joint probability density functions. Am Meteorol Soc 59:3519–3539
Lemone MA (1973) Modulation of turbulence energy by longitudinal rolls in an unstable planetary boundary layer. J Atmos Sci 33:1308–1320
Lemone MA, Pennell WT (1976) The relationship of trade wind cumulus distribution to subcloud layer fluxes and structure. Mon Weather Rev 104:524–539
Lewellen WS, Yoh S (1993) Binormal model of ensemble partial cloudiness. J Atmos Sci 50:1228–1237
Morcrette JJ, Smith L, Fouquart Y (1986) Pressure and temperature dependence of the absorption in longwave radiation parametrizations. Control Atmos Phys 59:455–469
Neggers RAJ (2009) A dual mass flux framework for boundary layer convection. Part 2: clouds. J Atmos Sci 66:1489–1506
Neggers RAJ, Siebesma P, Jonker HJJ (2002) A multiparcel model for shallow cumulus convection. J Atmos Sci 59:1655–1668
Neggers RAJ, Jonker HJJ, Siebesma AP (2003) Size statistics of cumulus clouds populations in large-eddy simulations. J Atmos Sci 60:1060–1074
Neggers RAJ, Stevens B, Neelin JD (2007) Variance scaling in shallow cumulus-topped mixed layers. Q J R Meteorol Soc 133:1629–1641
Neggers RAJ, Koehler M, Beljaars AMM (2009) A dual mass flux framework for boundary layer convection. Part 1: transport. J Atmos Sci 66:1465–1487
Pergaud J, Masson V, Malardel S, Couvreux F (2009) A parametrization of dry thermals and shallow cumuli for mesoscale numerical weather prediction. Boundary-Layer Meteorol 132:83–106
Perraud E, Couvreux F, Malardel S, Lac C, Masson V, Thouron O (2010) Evaluation of statistical distributions for the parametrization of subgrid boundary-layer clouds. Boundary-Layer Meteorol 140:263–294
Rio C, Hourdin F (2008) A thermal plume model for the convective boundary layer: representation of cumulus clouds. J Atmos Sci 65:407–425
Rio C, Hourdin F, Couvreux F, Jam A (2010) Resolved versus parametrized boundary layer thermals. Part II: continuous formulations of mixing rates for mass-flux schemes. Boundary-Layer Meteorol 135:469–483
Siebesma A, Teixera J (2000) An advection-diffusion scheme for the convective boundary layer, description and 1D results. In: Proceedings of 14th AMS symposium on boundary layers and turbulence. AMS, Boston
Siebesma AP, Bretherton CS, Brown A, Chlond A, Cuxart J, Duynkerke PG, Jiang H, Khairoutdinov M, Lewellen D, Moeng C-H, Sanchez E, Stevens B, Stevens DE (2003) A large eddy simulation intercomparison study of shallow cumulus convection. J Atmos Sci 60:1201–1219
Smith RNB (1990) A scheme for predicting layer clouds and their water content in general circulation model. Q J R Meteorol Soc 116:435–460

Soares P, Miranda P, Siebesma A, J T (2004) An eddy-diffusivity/mass flux parametrization for dry and shallow cumulus convection. Q J R Meteorol Soc 130:3365–3383

Sommeria G, Deardorff JW (1977) Subgrid-scale condensation in models of nonprecipitating clouds. J Atmos Sci 34:344–355

Tompkins AM (2002) A prognostic parametrization for the subgrid-scale variability of water vapor and clouds in large-scale models and its use to diagnose cloud cover. J Atmos Sci 59:1917–1942

Yamada T (1983) Simulations of nocturnal drainage flows by a q^2l turbulence closure model. J Atmos Sci 40:91–106